Advanced Composite Materials
Publication details, including instructions for authors and subscription information:
http://www.tandfonline.com/loi/tacm20

Simulation of Compression Effect on Filling Process in Compression Resin Transfer Molding

Chih-Yuan Chang [a]
[a] Department of Mechanical and Automation Engineering, Kao Yuan University, Lu-Chu, Taiwan 82101, R. O. C; t30044@cc.kyu.edu.tw
Version of record first published: 02 Apr 2012.

To cite this article: Chih-Yuan Chang (2011): Simulation of Compression Effect on Filling Process in Compression Resin Transfer Molding, Advanced Composite Materials, 20:2, 197-211

To link to this article: http://dx.doi.org/10.1163/092430410X547038

VSP

Advanced Composite Materials 20 (2011) 197–211

ADVANCED COMPOSITE MATERIALS
brill.nl/acm

Simulation of Compression Effect on Filling Process in Compression Resin Transfer Molding

Chih-Yuan Chang *

Department of Mechanical and Automation Engineering, Kao Yuan University, Lu-Chu, Taiwan 82101, R.O.C.

Received 11 August 2009; accepted 19 August 2010

Abstract

The compression resin transfer molding (CRTM) filling process involves two stages: the injection phase and the compression phase. Two injection modes are considered — constant volumetric flow rate and constant pressure — while the constant compression velocity is utilized in this study. Three typical cases are used to investigate the compression initiation effects on the filling process. When the inlet condition is a constant flow rate, the numerical results show that the compression has both increase and decrease effects on the inlet pressure. Thus, a discontinuity in the inlet pressure is present at the onset or the end of compression. Among three CRTM cases, the process with a simultaneous injection and compression end maximally reduces the inlet pressure by 80% but increases the mold filling time by 65% compared with the resin transfer molding (RTM). For the inlet condition being a constant pressure, the resin may flow out of the mold cavity through the inlet when an excessively low injection pressure and high compression speed are applied concurrently. Compared with RTM, the CRTM processes reduce the mold filling time by 68–76% but cannot ensure a reduction in inlet pressure.

Keywords

Compression resin transfer molding, filling process, simulation

Nomenclature (units)

dt Time interval (s)

h Cavity thickness (m)

h_{f} Final cavity thickness (m)

h_{i} Initial cavity thickness (m)

$\dot{h}$ Compression speed (m/s)

* E-mail: t30044@cc.kyu.edu.tw
Edited by the JSCM and KSCM

DOI:10.1163/092430410X547038

K Permeability of the fibrous reinforcement (m^2)

P Pressure (Pa)

P_{in} Fluid pressure at the inlet (Pa)

Q Volumetric flow rate (m^3/s)

r_f The radius of the flow front (m)

r_{in} The radius of the inlet (m)

S Curve of flow front

t Time (s)

t_{in} Injection time (s)

t_S Compression initiating time (s)

u, v Velocity components in x, y direction (m/s)

v_r Radial fluid velocity (m/s)

x, y Coordinate components in the physical domain (m)

Greek symbols

ξ, η Coordinate components in the computational domain

Φ Shape function

Ω, Ψ Control functions in the body-fitted method

ϕ Porosity

ϕ_i Initial porosity

μ Resin viscosity (Pa s)

1. Introduction

Over the years, several modifications of the resin transfer molding (RTM) process have been proposed to enhance the fiber volume fraction and reduce the mold filling time or molding pressure. One of the effective methods is to incorporate the method of compression into the RTM. This technology is called compression resin transfer molding (CRTM). In the process, resin is injected into a partial closed mold cavity filled with fibrous reinforcement known as a preform. Then the mold platens are brought together, driving the resin through the preform and compacting the laminate to the final cavity thickness.

Um *et al.* [1] proposed the similarity relations for pressure, resin velocity and flow front propagation in RTM to correlate another desired case from the already obtained numerical result. The efforts could be appreciably reduced since similar-

ity solutions were used instead of repeated numerical calculations. Ito *et al.* [2] proposed a smart manufacturing system for RTM. They utilized numerical simulation to predict the resin flow behavior and determine the preliminary process conditions. The injection pressure was controlled with a dielectric sensor, which monitored the resin flow front. Han *et al.* [3] proposed a numerical code to simulate the flow and heat transfer in injection/compression liquid composite molding (LCM). The flow in the runner and the fiber-free areas was simplified by using an equivalent permeability approach. They reported that the injection/compression LCM process could lead to more regular filling pattern and reduce the molding pressure significantly. Wirth and Gauvin [4] performed two series of plaque molding experiments in CRTM. In the first series, an open gap was present on the top of the preform. Thus the resin injection time was extremely short and most filling was elevated to the final closing of the cavity. In the second series, the injection and closing occurred simultaneously. They reported that the filling rate was much slower at the end of the filling process. Through a flow visualization experiment, Chang [5, 6] developed a theoretical model to simulate the filling process in injection/compression molding (I/CM) in which a gap existed above the preform. They pointed out that the gap resulted in a preferential flow during resin injection. Using small gap size and high compression speed could achieve the minimum mold filling time for the simultaneous I/CM process. Deleglise *et al.* [7] presented a method to study the material deformation in LCM. Three typical examples were used to cover the case of induced or forced deformations by using an open-source code, LIMS (Liquid Injection Molding Simulation). Pham *et al.* [8, 9] developed a CRTM filling algorithm based on resin conservation on a deformable grid to predict the flow front at each time step. The model allowed study of the effect of compression on the filling of a composite part for different compression speeds and injection pressures. The accuracy of the model was verified by comparing the numerical results with analytical solutions. Kang and Lee [10] also proposed a numerical code to predict the resin flow, temperature, pressure and degree of cure distribution during resin transfer/compression molding (RT/CM). The compression force required for squeezing the impregnated preform can be calculated. Experiments were performed for a three-dimensional shell to verify the feasibility of the RT/CM process and the numerical scheme. Bickerton and Abdullah [11] utilized analytical solutions of simple flow geometries to explore the potential benefits of I/CM relative to RTM. This model, based on elastic preform deformation, was used to investigate the effect of process on filling times, and clamping force requirements. They reported that the development of viscoelastic reinforcement deformation models was required to improve modeling of these processes. Shojaei [12] developed a three-dimensional numerical code to simulate the filling process by using control volume/finite element method (CV/FEM) in CRTM. An effective elastic modulus was introduced for multi-layer preforms connecting the mold closing speed to deformation rate of individual layers. Element characteristic height and element characteristic surface area were introduced to take into account irregular elements in the simulation. Bhat

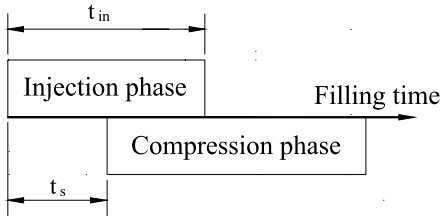

Special case: (1) Simultaneous CRTM, $t_S = 0$. (2) Sequential CRTM, $t_S = t_{in}$.

Figure 1. The relationship between the injection phase and the compression phase.

et al. [13] explored the CRTM process by assembling the process parameters into non-dimensional groups to reduce the number of variables. The impact of the dimensionless parameters on impregnation time is investigated with the numerical model.

Young and Chiu [14] reported that compression transfer molding (CTM) could reduce the mold filling time by 37–46% as compared to RTM. No major difference could be identified for the two sets of flexural strength for both RTM and CTM processes. Chang *et al.* [15] investigated the effects of process variables, including injection pressure, mold opening distance, resin temperature, compression pressure, pre-heated mold temperature and cure temperature, on the quality of CRTM products by applying Taguchi's method. They reported that the compression pressure and the resin temperature are significant variables for improvements in the mechanical properties of the part.

The objective of this research is to study a two-dimensional CRTM mold filling process. The resin flow in the fibrous preform is laminar and governed by Darcy's law during the filling process. While several numerical analyses have been presented previously, the compression initiation effects on the filling process have not been discussed. The flow model involving the body-fitted FEM is implemented to predict the resin front advancement and other relative properties. Simulations are also applied in RTM for comparison purposes.

2. Theory

2.1. Governing Equations

The CRTM mold filling process involves two stages: the injection phase and the compression phase. The relationship between the injection phase and the compression phase is shown in Fig. 1. The resin flow in the fibrous reinforcements is laminar and governed by Darcy's law:

$$u = -\frac{K}{\mu}\frac{\partial P}{\partial x}, \tag{1a}$$

$$v = -\frac{K}{\mu}\frac{\partial P}{\partial y}, \tag{1b}$$

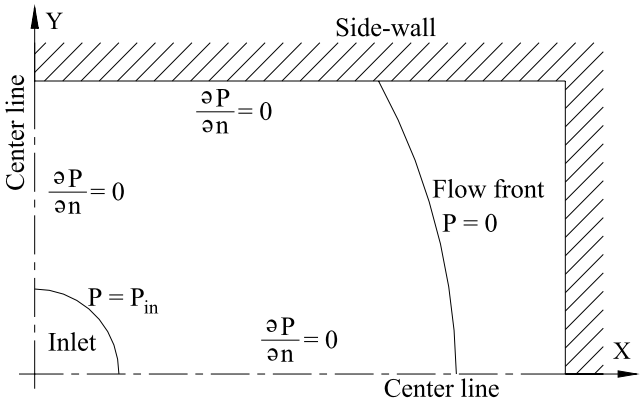

Figure 2. Physical domain and boundary conditions.

where P, u and v represent resin pressure and velocities in the x and y directions, respectively. K is the permeability of the preform and μ is the resin viscosity. The inverse of permeability describes the resistance offered by a fibrous preform to the flow of fluid. A thickness-averaged continuity equation has been applied:

$$\frac{\partial u}{\partial x} + \frac{\partial v}{\partial y} = -\frac{\dot{h}}{h}, \tag{2}$$

where h and $\dot{h}$ are the mold cavity thickness and compression speed, respectively. Note that $\dot{h}$ is negative during compression.

Combining Darcy's law, equation (1) and the continuity equation (2), the pressure equation is written as:

$$\frac{\partial}{\partial x}\left(-\frac{K}{\mu}\frac{\partial P}{\partial x}\right) + \frac{\partial}{\partial y}\left(-\frac{K}{\mu}\frac{\partial P}{\partial y}\right) = -\frac{\dot{h}}{h}. \tag{3}$$

Solving equation (3) with appropriate boundary conditions the resin pressure can be determined. The boundary conditions are shown in Fig. 2. For a rectangular mold, only one-quarter of the mold cavity needs to be considered since the physical domain is symmetric about the x- and y-axes.

Notice that the inlet pressure varies with mold filling time for a constant flow rate injection, while it is invariable for a constant injection pressure. After enough resin is injected, the injection flow rate needs to be switched to null. That is, the boundary condition turns into $\partial P/\partial n = 0$ at the inlet.

The volumetric flow rate (Q) is calculated by integrating resin across the surface of the flow front:

$$Q = \oint (u\vec{i} + v\vec{j}) \cdot h \, \mathrm{d}\vec{S}, \tag{4}$$

where $\vec{S}$ represent the curve of the flow front, respectively.

2.2. Porosity

The thickness of the mold cavity is variable in CRTM. That is, the porosity of the fibrous preform is a function of mold filling time. In this study a constant velocity in closing the mold is applied during compression. For a two-dimensional mold, the porosity (ϕ) can be calculated at any given time as follows:

$$\phi = \frac{h_{\mathrm{i}} \times \phi_{\mathrm{i}} - |\dot{h}|(t - t_{\mathrm{S}})}{h_{\mathrm{i}} - |\dot{h}|(t - t_{\mathrm{S}})}, \tag{5}$$

where h_{i} and ϕ_{i} are the initial cavity thickness and the initial porosity, respectively; t_{S} is the compression initiating time. The random fiber mat (TGFM-300P/E) is utilized in the present study. The empirical relation between the permeability and the porosity is provided as below [16]:

$$K = 1.722 \times 10^{-15} \times \exp(15.771 \times \phi)\ \mathrm{m}^2, \quad 0.695 \leqslant \phi \leqslant 0.867. \tag{6}$$

3. Numerical Procedure

One of the difficulties of simulating the CRTM filling stage is the numerical treatment of the moving and irregular front surface of the resin. The body-fitted FEM, the combination of body fitted grid generation with the FEM, provides numerous advantages such as uniformly spaced grids, easy application of surface boundary conditions and modular technique, etc. It is well suited to solve the free moving boundary problem.

3.1. Galerkin's Method

In the present FEM model, the method of weight residual adopts the Galerkin method. The Galerkin residual equation for governing equation (3) can be derived from

$$\begin{aligned} &\iint \left(\frac{\partial}{\partial x}\left(-\frac{K}{\mu}\frac{\partial P}{\partial x} \right) + \frac{\partial}{\partial y}\left(-\frac{K}{\mu}\frac{\partial P}{\partial y} \right) \right) \Phi_j \,\mathrm{d}x\,\mathrm{d}y \\ &\quad = \iint \left(-\frac{\dot{h}}{h} \right) \Phi_j \,\mathrm{d}x\,\mathrm{d}y, \quad j = 1, 2, \ldots, 6, \end{aligned} \tag{7}$$

where Φ_j is the shape function or trial function. The element applied in the present simulation is the quadratically interpolated triangular element with six nodes — three at the vertices and three at the middle of each side. The corresponding shape functions are

$$\begin{aligned} \Phi_1(\xi, \eta) &= (1 - (\xi + \eta))(1 - 2(\xi + \eta)), \\ \Phi_2(\xi, \eta) &= \xi(2\xi - 1), \\ \Phi_3(\xi, \eta) &= (2\eta - 1), \\ \Phi_4(\xi, \eta) &= 4\xi(1 - (\xi + \eta)), \\ \Phi_5(\xi, \eta) &= 4\xi\eta, \\ \Phi_6(\xi, \eta) &= 4\eta(1 - (\xi + \eta)), \end{aligned} \tag{8}$$

where ξ and η are the local coordinates for each element. Integrating equation (7) by parts and applying boundary conditions into the equation, the pressure distribution can be calculated numerically.

3.2. Nodal Coordinates

In the body-fitted method, a set of elliptic partial differential equations is used as follows [17]:

$$\xi_{xx} + \xi_{yy} = \Omega(\xi, \eta)\left(\xi_x^2 + \xi_y^2\right), \tag{9a}$$

$$\eta_{xx} + \eta_{yy} = \Psi(\xi, \eta)(\eta_x^2 + \eta_y^2), \tag{9b}$$

where Ω and Ψ are the control functions. Interchanging the dependent variables (ξ, η) with the independent variables (x, y) in the above equations yields:

$$a(x_{\xi\xi} + \Omega x_\xi) - 2bx_{\xi\eta} + c(x_{\eta\eta} + \Psi x_\eta) = 0, \tag{10a}$$

$$a(y_{\xi\xi} + \Omega y_\xi) - 2by_{\xi\eta} + c(y_{\eta\eta} + \Psi y_\eta) = 0, \tag{10b}$$

where $a = x_\eta^2 + y_\eta^2$, $b = x_\xi x_\eta + y_\xi y_\eta$ and $c = x_\xi^2 + y_\xi^2$. The control functions, based on the assumptions that the curvature along the geometric boundaries is locally zero and the grid lines are orthogonal to each other in the vicinity of geometric boundaries, are determined by

$$\Omega = -(x_{\xi\xi}x_\xi + y_{\xi\xi}y_\xi)/\left(x_\xi^2 + y_\xi^2\right), \tag{11a}$$

$$\Psi = -(x_{\eta\eta}x_\eta + y_{\eta\eta}y_\eta)/\left(x_\eta^2 + y_\eta^2\right) \tag{11b}$$

along the geometric boundaries. For the interior points, the control function is interpolated from that on the geometric boundaries. The form of equations (10) in the finite difference method (FDM) is

$$\begin{aligned} &a(R_{i+1,j} - 2R_{i,j} + R_{i-1,j} + \Omega(R_{i+1,j} - R_{i-1,j})/2) \\ &\quad - 2b(R_{i+1,j+1} - R_{i-1,j+1} + R_{i+1,j-1} + R_{i-1,j-1})/4 \\ &\quad + c(R_{i,j+1} - 2R_{i,j} + R_{i-1,j} + \Psi(R_{i,j+1} - R_{i,j-1})/2) = 0, \end{aligned} \tag{12}$$

where R can be x or y. The nodal coordinates are updated for each time step. In order to save computational time, the numbers of element are proportional to the volume of filled liquid. An auto-transformation of numbering of nodes between the body-fitted FDM and FEM is necessary in the pre-process of the FEM. Thus the body-fitted FEM is an auto-meshed scheme.

3.3. Numerical Procedure

During the filling process, the resin progression can be calculated as follows:

1. Set the injection and compression parameters.
2. Guess the position of the flow front by the formula of $R_n = R_{n-1} + V_{n-1} \times dt$. R_{n-1} and R_n denote the front position in the $(n-1)$th and nth time step, respectively. V_{n-1} is the front velocity in the $(n-1)$th time step. dt is the time interval.

3. Generate the mesh and number of the element by the body-fitted FEM.
4. Calculate the velocity and pressure fields.
5. Update the position of the flow front by the formula of $R_{n-1} + dt \times (V_{n-1} + V_n)/2$. V_n is the front velocity in the nth time step. Repeat steps 2 to 5 until the flow front converges to the correct position.
6. Check the injection resin quantity. After enough resin is injected, the inlet is closed.
7. Repeat steps 1 to 6 until the mold filling process finishes.

The FEM code of Burnett [18] is modified and utilized in the present simulation.

4. Results and Discussion

In the present paper, two injection modes are considered, constant volumetric flow rate and constant pressure; while constant velocity in closing the mold is taken as the compression condition during the CRTM mold filling process. Three typical cases are used to investigate the compression initiation effects on the filling process. The planar dimensions of a rectangular cavity are 0.20 m × 0.12 m. The cavity thickness can vary from 0.0075 m to 0.004 m and the corresponding porosities of the preform are 0.82 and 0.7. The inlet is located at the center of the mold cavity with a radius of 0.005 m. The density and viscosity of the resin system (Araldite LY564 and hardener HY2962) are about 1105 kg/m^3 and 0.5 Pa s at room temperature.

4.1. Constant Volumetric Flow Rate

Owing to the isotropy of the fibrous preform, the fluid expands radially before the fluid meets the side walls. By rewriting equation (3) in polar coordinates, the pressure gradient in the flow region can be deduced as follows [8]:

$$\frac{\mathrm{d}P}{\mathrm{d}r} = \frac{\mu\dot{h}}{2Kh}r - \left(\frac{\mu Q}{2\pi Kh} + \frac{\mu\dot{h}}{2Kh}r_{\mathrm{in}}^2\right)\frac{1}{r}, \tag{13}$$

where r_{in} denotes the radius of the inlet. The pressure gradient needs to be negative at any given position in order that the resin flow is directed into the mold cavity.

According to equation (4), the relationship between the radial flow velocity (v_{r}) and the mold filling time in polar coordinates can be written as:

$$v_{\mathrm{r}} = \frac{Q}{2\pi r_{\mathrm{f}}h} = \frac{Q}{2\pi r_{\mathrm{f}}(h_{\mathrm{i}} - |\dot{h}|(t - t_{\mathrm{S}}))} = \phi\frac{\mathrm{d}r_{\mathrm{f}}}{\mathrm{d}t}, \tag{14}$$

where r_{f} denotes the radius of the flow front. This equation interprets that the compression action can make the flow front advance faster as a result of the reduction in cavity thickness. Using equation (5) and integrating equation (14) from the inlet

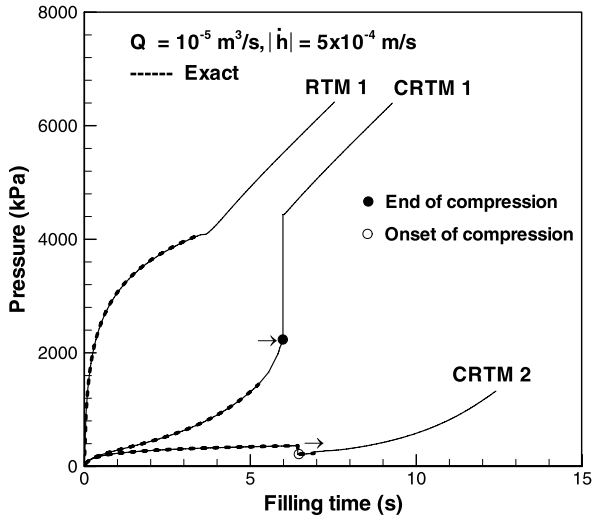

Figure 3. The variation in fluid pressure at the inlet during the filling stage.

radius and time $t = 0$, to the radius of the flow front and time $t = t$, the relation between the flow front radius *versus* mold filling time can be obtained:

$$r_f = \sqrt{r_{in}^2 + \frac{Q \times t_S}{\pi \phi_i h_i} + \frac{Q}{\pi |\dot{h}|} \ln \frac{\phi_i h_i}{\phi_i h_i - |\dot{h}|(t - t_S)}}. \tag{15}$$

Integrating equation (13) and substituting equation (15), the exact inlet pressure can be determined as below:

$$P_{in} = \frac{\mu Q}{2\pi K h} \ln \frac{r_f}{r_{in}} + \frac{\mu \dot{h}}{K h} \left(\frac{r_f^2}{2} \ln \frac{r_f}{r_{in}} + \frac{r_{in}^2 - r_f^2}{4} \right). \tag{16}$$

Apparently the first term at the right-hand side of equation (16) is positive and the other is negative due to $\dot{h}$. Recall that $h = h_i - |\dot{h}| \times (t - t_S)$. Thus, the compression has both increase and decrease effects on the inlet pressure and they are comparable. The increase in inlet pressure is always dominant because the inlet pressure is greater than zero. Figure 3 shows the variation in fluid pressure at the inlet during the filling stage. A good agreement is observed between the numerical prediction and the exact solution denoted by a dashed line, as shown in Fig. 3.

For the CRTM 1 case, it is a simultaneous CRTM filling process. The injection is longer than compression, so the injection continues after the compression ends. The compression time equals $(h_i - h_f)/|\dot{h}|$ for the constant compression velocity where h_f is the final cavity thickness. Injection and compression are performed simultaneously, while the inlet pressure rises because the total friction between the fluid and the preform increases as the resin saturation zone increases. After the compression ends the filling process is identical to RTM. A jump in inlet pressure is found at the end of compression because of the lack of a compression decrease effect. After that, the inlet pressure shows an approximately linear increase since

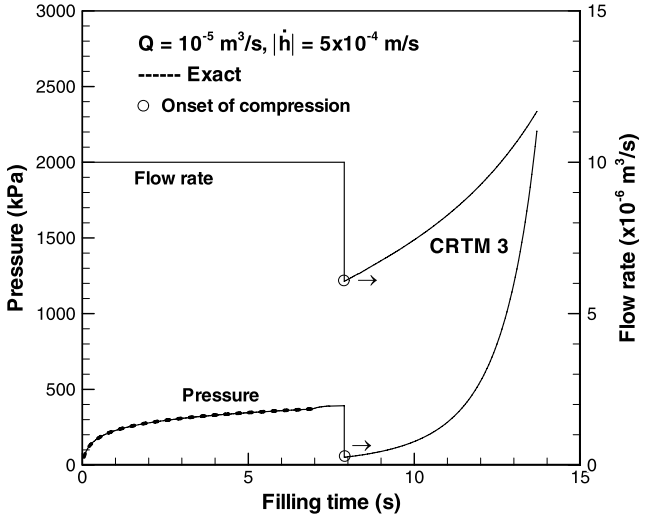

Figure 4. The variation in inlet pressure and volumetric flow rate during the filling stage.

the filling behavior is nearly unidirectional in the late filling process. The RTM can be regarded as a special simultaneous CRTM process with infinity compression velocity. As we can expect, the final inlet pressures in RTM 1 and CRTM 1 are equal since the flow resistances offered by the preform are the same at the completion of filling. The compression history does not affect the finial inlet pressure.

For the CRTM 2 case, the compression initiates at the injection time of 6.43 s, and then injection and compression concur simultaneously until the completion of the filling process. Before compression, the filling process is equivalent to RTM with a higher cavity thickness and consequently possesses a lower inlet pressure. The inlet pressure falls at the onset of compression due to the compression decrease effect. After that, the inlet pressure rises gradually and the trend is similar to that in the early CRTM 1 filling process.

Figure 4 shows the variation in inlet pressure and flow rate for the CRTM 3 case. It is a sequential CRTM filling process. Before compression the inlet pressure is identical to that in CRTM 2. After enough resin is injected, the inlet is closed and the filling process turns into compression molding. The inlet pressure and volumetric flow rate rapidly drop off at the instant when the inlet condition is switched. The compression action can keep the resin flowing and cause the inlet pressure to rise. Note that the flow rate cannot be maintained constant during compression molding. This can be explained by the fact that the saturated preform area squeezed by the mold platen increases with the compression time. Thus, a great amount of resin flows out for a thickness reduction. A comparison of CRTM cases indicates that CRTM 2 possesses the minimum highest inlet pressure due to the compression effect on the late injection phase. CRTM 2 reduces the inlet pressure by 80% but increases the mold filling time by 65% as compared with the RTM process. The

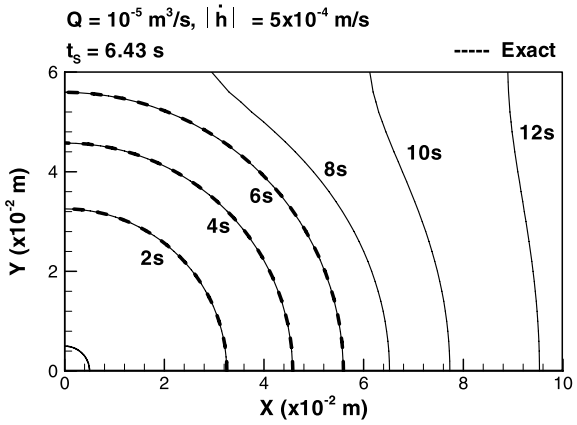

Figure 5. The flow front of the resin at various times for the CRTM 2 case.

simultaneous CRTM possesses the shortest mold filling time but the highest inlet pressure. Compared with RTM, the CRTM process cannot reduce the mold filling time but may produce a marked reduction in inlet pressure.

Figure 5 shows the flow front of the resin at various times for the CRTM 2 case. As stated above, the flow behaviour is radial in the early filling process. After the resin meets the side wall, the radial flow gradually transforms into a unidirectional flow due to side wall confinement.

4.2. Constant Injection Pressure

As an alternative, a constant pressure can be utilized in the injection phase. The minimum highest inlet pressure in the constant flow rate case (CRTM 2) is taken as the injection pressure. The compression speed remains the same. During the radial flow period the pressure gradient in polar coordinates can be deduced as follows [8]:

$$\frac{\mathrm{d}P}{\mathrm{d}r} = \frac{\mu\dot{h}}{2Kh}r - \left(r\ln\frac{r_\mathrm{f}}{r_\mathrm{in}}\right)^{-1}\left(P_\mathrm{in} - \frac{\mu\dot{h}}{4Kh}\left(r_\mathrm{in}^2 - r_\mathrm{f}^2\right)\right). \tag{17}$$

The negative pressure gradient at the inlet drives the resins flowing into the cavity when the injection pressure is larger than $(\mu\dot{h})/(4Kh)(r_\mathrm{in}^2 - r_\mathrm{f}^2 + 2r_\mathrm{in}\ln(r_\mathrm{f}/r_\mathrm{in}))$. This implies that an admissible minimum injection pressure exists. It relates to the resin viscosity, preform permeability (porosity), resin flow distance, compression speed and increases with the mold filling time. Generally, a reversed flow at the inlet can occur when an excessively low injection pressure and high compression speed are applied concurrently.

Figure 6 shows the variation in volumetric flow rate during the filling stage. In the plot, CRTM 4 and CRTM 6 are simultaneous and sequential CRTM processes. CRTM 5 is the compression initiation at the injection time of one second. In the CRTM cases, a high volumetric flow rate results in a short injection phase because of the high pressure gradient and large preform permeability in the early filling

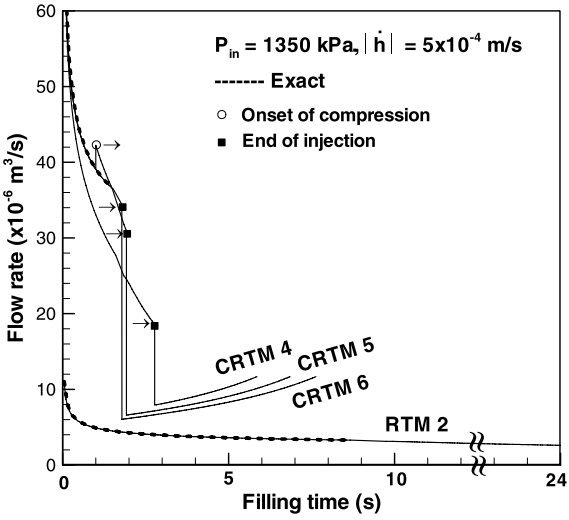

Figure 6. The variation in volumetric flow rate during the filling stage.

process. A jump in the flow rate occurs at the onset of compression in CRTM 5 due to the compression initiation. Once enough resin is injected, the volumetric flow rate rapidly falls due to the switch in inlet condition. After that, the filling process turns into compression molding and the variation in flow rate is similar to that in CRTM 3 compression molding. A comparison of RTM 2 and CRTM cases is performed. After the compression initiation, the injection flow rate decreases as a result of the increase in flow resistance offered by the preform. However, the sequential CRTM does not possess the least mold filling time because the high flow rate phase (injection phase) is too short. The simultaneous CRTM possesses the shortest filling time. Similarly, the final flow rates in CRTM cases are equal. The injection history does not affect the finial flow rate. Compared with RTM 2, the CRTM processes reduce the mold filling time by 68–76% but cannot ensure a reduction in inlet pressure as shown in Fig. 7. This is because the inlet pressure is dependent on the compression speed in compression molding.

Table 1 shows the mold filling time and maximum inlet pressure for all RTM and CRTM processes. By grading the data, the CRTM 4 is an appropriate process for the present mold filling.

5. Conclusions

A two-dimensional numerical model of the CRTM filling process was presented in this study. Two injection modes were considered — a constant flow rate and constant pressure — while constant velocity in closing the mold was taken as the compression condition. Three typical cases were used to investigate various compression initiating times on the filling process. The simulation was based on the body-fitted FEM.

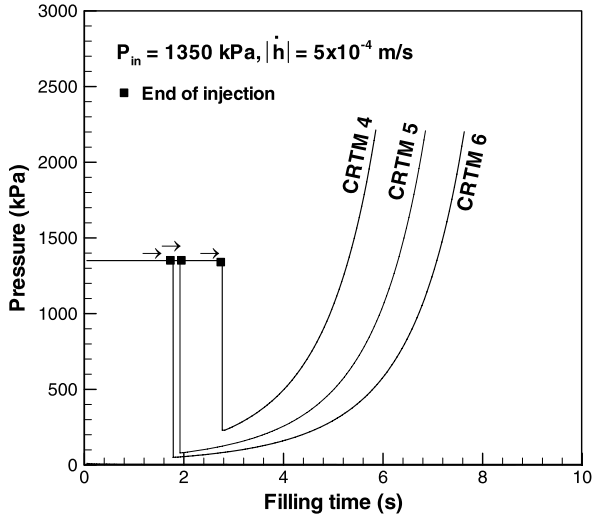

Figure 7. The variation in inlet pressure and flow rate during the filling stage.

Table 1.
The mold filling time and maximum inlet pressure for all RTM and CRTM processes

Process	Filling time	Maximum inlet pressure	Characteristics
Constant volumetric flow rate ($Q = 10^{-5}$ m^3/s)			
RTM 1	7.5 s	6400 kPa	High injection pressure and medium filling time
CRTM 1	9.3 s	6400 kPa	High injection pressure and medium filling time
CRTM 2	12.4 s	1350 kPa	Low injection pressure and long filling time
CRTM 3	13.7 s	2200 kPa	Medium inlet pressure and long filling time
Constant injection pressure ($P_{\text{in}} = 1350$ kPa)			
RTM 2	24.1	1350	Low injection pressure and long filling time
CRTM 4	5.9	2200	Medium inlet pressure and short filling time
CRTM 5	7.6	2200	Medium inlet pressure and medium filling time
CRTM 6	6.9	2200	Medium inlet pressure and medium filling time

When the inlet condition was taken as a constant flow rate, the compression was verified to have both increase and decrease effects on the inlet pressure using the analytical solution. This accounts for the discontinuity in inlet pressure at the onset or the end of compression. Compared with RTM, the CRTM cases may have a strong reduction in inlet pressure but cannot reduce the mold filling time. Among the CRTM cases, the simultaneous end of injection and compression case can reduce the highest inlet pressure maximally. The simultaneous CRTM possesses the shortest mold filling time but the highest inlet pressure. The highest inlet pressures in simultaneous CRTM and RTM are equal. The compression history does not affect the inlet pressure at the completion of the filling process.

When the inlet condition is a constant injection pressure, a high injection flow rate is a common feature in the CRTM injection phase. Note that an admissible minimum injection pressure exists and relates to the resin viscosity, preform permeability (porosity), resin flow distance and compression speed. A reversed flow at the inlet usually occurs when an excessively low injection pressure and high compression speed are applied concurrently. A comparison of RTM and CRTM indicated that all CRTM cases can significantly reduce the mold filling time but cannot ensure a reduction in inlet pressure, which is dependent on the compression speed in the compression phase. Among the CRTM cases, the simultaneous CRTM possessed the least mold filling time.

In summary, while a reduction in inlet pressure can be achieved, these gains may be balanced by increased mold filling time and *vice versa*. By grading the processes, the simultaneous CRTM with a constant injection pressure is appropriate for the present mold filling process.

References

1. M. K. Um, J. H. Byun and I. M. Daniel, Similarity relations of resin flow in resin transfer molding process, *Adv. Compos. Mater.* **18**, 135–152 (2009).
2. T. Ito, K. Yamagishi, I. Okumura, S. Kitade and Y. Shigegaki, Smart manufacturing of low-cost integrated panel by resin-transfer molding, *Adv. Compos. Mater.* **13**, 57–66 (2004).
3. K. Han, J. Ni, J. Toth, L. J. Lee and J. P. Greene, Analysis of an injection/compression liquid composite molding process, *Polym. Compos.* **19**, 487–496 (1998).
4. S. Wirth and R. Gauvin, Experimental analysis of mold filling in compression resin transfer molding, *J. Reinf. Plast. Compos.* **17**, 1414–1430 (1998).
5. C. Y. Chang, Modeling of the filling process of resin injection/compression molding, *Adv. Compos. Mater.* **16**, 207–221 (2007).
6. C. Y. Chang, Simulation of mold filling in simultaneous resin injection/compression molding, *J. Reinf. Plast. Compos.* **25**, 1255–1268 (2006).
7. M. Deleglise, C. Binetruy and P. Krawczak, Simulation of LCM processes involving induced or forced deformations, *Composites Pt. A — Appl. Sci. Manuf.* **37**, 874–880 (2006).
8. X. T. Pham and F. Trochu, Simulation of compression resin transfer molding to manufacture thin composite shell, *Polym. Compos.* **20**, 436–459 (1999).
9. X. T. Pham, F. Trochu and R. Gauvin, Simulation of compression resin transfer molding with displacement control, *J. Reinf. Plast. Compos.* **17**, 1525–1556 (1998).
10. M. K. Kang and W. I. Lee, Analysis of resin transfer/compression molding process, *Polym. Compos.* **20**, 293–304 (1999).
11. S. Bickerton and M. Z. Abdullah, Modeling and evaluation of the filling stage of injection/compression moulding, *Compos. Sci. Technol.* **63**, 1359–1375 (2003).
12. A. Shojaei, Numerical simulation of three-dimensional flow and analysis of filling process in compression resin transfer moulding, *Composites Pt. A — Appl. Sci. Manuf.* **37**, 1434–1450 (2006).
13. P. Bhat, J. Merotte, P. Simacek and S. G. Advani, Process analysis of compression resin transfer molding, *Composites Pt. A — Appl. Sci. Manuf.* **40**, 431–441 (2009).

14. W. B. Young and C. W. Chiu, Study on compression transfer molding, *J. Compos. Mater.* **29**, 2180–2191 (1995).
15. C. Y. Chang, L. W. Hourng and T. Y. Chou, Effect of process variables on the quality of compression resin transfer molding, *J. Reinf. Plast. Compos.* **25**, 1027–1037 (2006).
16. C. J. Wu, L. W. Hourng and J. C. Liao, Numerical and experimental study on the edge effect of resin transfer molding, *J. Reinf. Plast. Compos.* **14**, 694–722 (1995).
17. P. D. Thomas and J. F. Middlecoff, Direct control of the grid point distribution in meshes generated by elliptic equation, *AIAA J.* **18**, 652–656 (1980).
18. D. S. Burnett, *Finite Element Analysis*. Addison-Wesley Publishing Company, Singapore (1988).